1-28-2011

Incoherent Scatter Radar Estimation of F Region Ionospheric Composition During Frictional Heating Events

M. Zettergren
Embry-Riddle Aeronautical University, zettergm@erau.edu

J. L. Semeter
Boston University

C. Heinselman
SRI International

M. Diaz
University of Chile

Scholarly Commons Citation

Zettergren, M., J. Semeter, C. Heinselman, and M. Diaz (2011), Incoherent scatter radar estimation of F region ionospheric composition during frictional heating events, J. Geophys. Res.,116, A01318.

Incoherent scatter radar estimation of *F* region ionospheric composition during frictional heating events

M. Zettergren,[1] J. Semeter,[2] C. Heinselman,[3] and M. Diaz[4]

Received 17 August 2010; revised 9 November 2010; accepted 15 November 2010; published 28 January 2011.

[1] A method is developed for estimating *F* region ion composition from incoherent scatter radar (ISR) measurements during times of frictional ion heating. The technique addresses ion temperature-mass ambiguities in the IS spectra by self-consistently modeling ion temperature profiles, including the effects of ion temperature anisotropies and altitude-independent neutral winds. The modeled temperature profiles are used in a minimization procedure to estimate ion composition consistent with the recorded IS spectra. The proposed method is applicable to short-integration (<5 min) data sets from either single-beam or multiple-beam experiments. Application of the technique to Sondrestrom ISR measurements shows increases in *F* region molecular ions in response to frictional heating, a result consistent with previous theoretical and observational work. Estimates of ion composition are shown to be relatively insensitive to moderate variations in the neutral atmospheric model, which serves as input to the method. The technique developed in this work is uniquely qualified for studying highly variable ion composition near auroral arcs and associated processes such as molecular ion upflows. It also addresses a systematic source of error in standard ISR analysis methods when they are applied in such situations.

Citation: Zettergren, M., J. Semeter, C. Heinselman, and M. Diaz (2011), Incoherent scatter radar estimation of *F* region ionospheric composition during frictional heating events, *J. Geophys. Res.*, *116*, A01318, doi:10.1029/2010JA016035.

1. Introduction

[2] Incoherent scatter radar (ISR) is one of the most powerful remote sensing tools for examining the high-latitude ionosphere. Transmitted radio waves are scattered by the ionospheric plasma and received by the ISR. The received signal covers a spectrum of frequencies, and ionospheric plasma parameters are estimated by fitting a theoretical model to this IS spectrum. Roughly speaking, the spectral width of the ion line component of the IS spectrum yields an estimate of T_i/m_i (ion temperature to mass ratio), the ion line peak to valley ratio gives T_e/T_i (electron to ion temperature ratio), the bulk ion line doppler shift gives v_i (line-of-sight drift velocity), and the total scattered power gives n_e (electron density). Unless extremely high-quality data exist, ion composition must be assumed in order to compute absolute ion and electron temperatures [*Evans*, 1969; *Oliver*, 1979; *Lathuillere et al.*, 1983]. At the Sondrestrom ISR facility (of interest to the present work), a static ion composition profile is generally used to process IS spectra.

[3] The importance of properly accounting for compositional changes in the auroral *F* region has been pointed out by many authors [cf. *Zettergren et al.*, 2010, and references therein]. One major source of ion composition variability is changes in chemical balance in the ionosphere due to highly temperature-sensitive reaction rates. At high latitudes electric fields drive the ionospheric plasma through the neutral atmosphere causing intense frictional heating. Resulting high ion temperatures *drastically* modify ion chemical reaction rates and generally favor conversion of O^+ to NO^+ [*McFarland et al.*, 1973; *Torr et al.*, 1977; *St.-Maurice and Torr*, 1978; *St.-Maurice and Laneville*, 1998] through the reaction

$$O^+ + N_2 \rightarrow NO^+ + N. \quad (1)$$

[4] This process can produce substantial amounts of molecular ions in the *F* region, creating severe alterations in ionospheric composition at high latitudes. Composition variability has been modeled in past work [e.g., *Schunk et al.*, 1975; *Diloy et al.*, 1996; *Zettergren et al.*, 2010], but has yet to be accounted for, in a definitive way, in high-latitude ISR data analysis.

[5] Various data processing strategies have been developed to mitigate ion temperature-mass ambiguities in IS spectra. Many of these methods rely on reduced parameter descriptions of the ionospheric density, temperatures, and

[1]Physical Sciences Department, Embry-Riddle Aeronautical University, Daytona Beach, Florida, USA.
[2]Department of Electrical and Computer Engineering and Center for Space Physics, Boston University, Boston, Massachusetts, USA.
[3]SRI International, Menlo Park, California, USA.
[4]Electrical Engineering Department, University of Chile, Santiago, Chile.

0148-0227/11/2010JA016035

composition, vs. altitude. *Oliver* [1979] developed such a method for midlatitudes that specified physical constraints for temperature and composition profiles for use in fitting IS spectra. Other, more recent, research has extended these ideas for use at high latitudes. *Cabrit and Kofman* [1997] developed a full profile technique, along with a parameterization of the composition profile, which was used to study diurnal and seasonal variations in ion composition [*Litvine et al.*, 1998]. The method proposed by these authors relied on the simultaneous analysis of both coded pulse and long pulse data. A similar technique and results were presented by *Shibata et al.* [2000]. Such methods produced reliable results for times when the ionosphere is undisturbed by strong electric fields and frictional heating.

[6] When the ionosphere is severely disturbed by electric fields, the reliable analysis of ISR data becomes extremely difficult [e.g., *Lathuillere and Kofman*, 2006]. This difficulty is mostly due to the dynamic nature of composition variability [*Zettergren et al.*, 2010] and the fact that ion temperature anisotropies [e.g., *St.-Maurice and Schunk*, 1979] further complicate the analysis [*Raman et al.*, 1981; *Hubert and Lathuillere*, 1989; *Lathuillere et al.*, 1991]. Several approaches have been developed for dealing with situations of intense ion heating. *Lathuillere et al.* [1983] found that, with sufficient integration time (~5 min), composition and ion temperature could be simultaneously extracted from the spectra, provided that a good initial guess is input into the estimation procedure. Other methods have relied on specifying either the electron temperature or ion temperature and fitting the IS spectra for composition. *Kelly and Wickwar* [1981] specified electron temperature by interpolating between reliable data points and used the results to estimate ion temperature and composition. *Häggström and Collis* [1990] used a model of ion heating to specify ion temperature for use in fitting the spectra for composition. Their method relied on electric field estimates from tristatic EISCAT measurements. *Gaimard et al.* [1996] also incorporated a model of ion heating into analysis of EISCAT data, reformulating the spectral estimation problem into one of finding $|\mathbf{v}_i - \mathbf{u}_n|$ (ion-neutral differential drift speed), n_e, T_e, p (ion composition parameter), and T_n (neutral temperature). Their analysis revealed that only 3 of these parameters could be reliably determined simultaneously with an automated method.

[7] Some authors have used complex models of ionospheric chemistry and transport to specify ion composition profiles to fitting routines [*Blelly et al.*, 1996; *Jenkins et al.*, 1997]. Direct modeling of ion composition works in situations of extended heating, but when the heating is highly variable the time history of the plasma must be known to properly calculate ion composition [*Zettergren et al.*, 2010]. This is due to the fact that once ion composition is altered, it can remain disturbed for long periods of time and convect to other latitudes and local times. The approaches and studies outlined above have, in general, confirmed the correlation of molecular ion densities in the F region with intense electric fields (a conclusion well supported in related theoretical work).

[8] The present work develops and evaluates a methodology to estimate ion composition during dynamic electric field disturbances occurring in time scales of < 5 min. Preference is given to methods applicable to single-radar, single-beam-position ISR experiments that constitute a significant number of past experiments. Such goals immediately restrict possible approaches to those of specifying ion or electron temperature in some way and fitting the ISR data for ion composition. Uncertainties in data sets with short integration times (< 5 min) are too large to attempt direction estimation of temperatures and composition simultaneously. Additional requirements are to account for ion temperature anisotropies, well documented in regions of strong electric fields [*Gaimard et al.*, 1996; *Hubert et al.*, 1996], and to deal with the considerable effects that neutral winds have on ion frictional heating [*St.-Maurice et al.*, 1999].

2. Estimation Technique

[9] The approach taken in this work is to model line-of-sight ion temperatures self-consistently using indirect observations of the effective electric field (which implicitly include some neutral wind effects). Discrepancies between a self-consistently modeled ion temperature profile and the corresponding fitted profile are interpreted in terms of errors in the ion composition assumed by the fitter. The composition is estimated as that which brings the model results and data into best agreement. The method outlined here is an extension and refinement of the author's dissertation research [*Zettergren*, 2009] and an implementation of the method proposed by *Zettergren et al.* [2010].

2.1. Modeling Temperature Profiles of O^+ and NO^+

[10] Ion temperature at high latitudes is controlled by frictional heating from $\mathbf{E}_\perp \times \mathbf{B}$ drift of the ionospheric plasma and heat exchange with the neutral atmosphere. Below ~350 km ion energy balance equations may be simplified to yield an expression for the parallel temperature for ion species s [*St.-Maurice et al.*, 1999]:

$$T_{s\parallel} = T_n + \frac{3}{2}\beta_{s\parallel}\frac{\langle m_n\rangle}{3k_B}\frac{1}{1+(\nu_s/\Omega_s)^2}\left(\frac{E'_\perp}{B}\right)^2. \tag{2}$$

[11] In equation (2), T_n is the neutral temperature, $\beta_{s\parallel}$ is a collision-type-dependent coefficient which describes temperature anisotropies [*Winkler et al.*, 1992; *McCrea et al.*, 1993], $\langle m_n\rangle$ is an average mass of the neutral atmospheric constituents [e.g., *Winkler et al.*, 1992], k_B is the Boltzmann constant, ν_s is the ion-neutral collision frequency, Ω_s is the gyrofrequency, and B is the geomagnetic field strength. Neutral atmospheric parameters in equation (2) are taken from the NRLMSISE-00 model [*Picone et al.*, 2002], and the $\beta_{s||}$ factor is taken from a synthesis of theoretical calculations by *Winkler et al.* [1992] and observations by *McCrea et al.* [1993]. $E'_\perp$ is the effective electric field strength defined by the electric field in a frame of reference drifting with the neutral gas:

$$\mathbf{E}'_\perp = \mathbf{E}_\perp + \mathbf{u}_{n\perp} \times \mathbf{B}, \tag{3}$$

where $\mathbf{E}_\perp$ is the electric field in an Earth-fixed frame of reference and $\mathbf{u}_{n\perp}$ is the neutral wind velocity. Using the above quantities, the ion temperature may be modeled from equation (2) provided the effective electric field can be measured or estimated (see section 2.2).

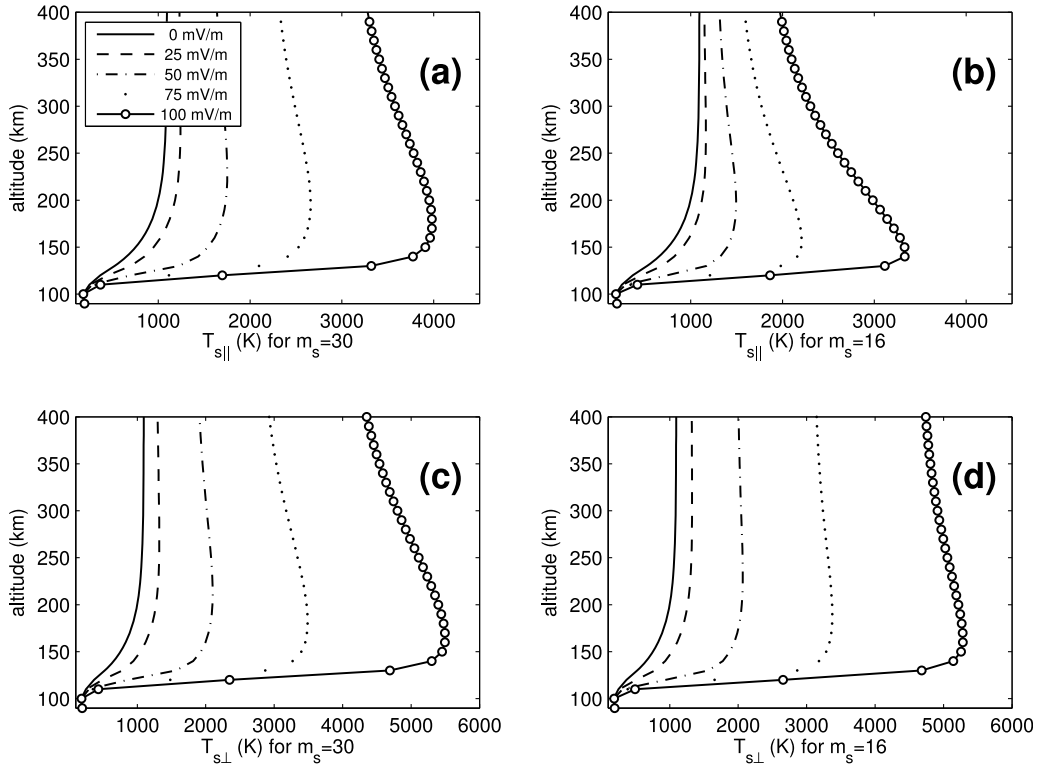

Figure 1. O^+ and NO^+ parallel and perpendicular temperature for various values of the effective electric field: (a) parallel NO^+ temperature, (b) parallel O^+ temperature, (c) perpendicular NO^+ temperature, and (d) perpendicular O^+ temperature.

[12] In the auroral zone, ion temperatures parallel to the magnetic field differ substantially from perpendicular temperatures [*St.-Maurice and Schunk*, 1979]. In these cases modeling of both parallel and perpendicular temperatures is necessary. The perpendicular temperature in the ionosphere below ~ 350 km, for species s, is given by an expression similar in form to the parallel temperature [*Winkler et al.*, 1992]:

$$T_{s\perp} = T_n + \frac{3}{2}\beta_{s\perp}\frac{\langle m_n\rangle}{3k_B}\frac{1}{1+(\nu_s/\Omega_s)^2}\left(\frac{E'_\perp}{B}\right)^2. \quad (4)$$

[13] Figure 1 shows the results of modeling species ion temperatures using equations (2) and (4) with various values of the effective electric field. Figures 1a and 1b show parallel temperatures for NO^+ and O^+, while Figures 1c and 1d show perpendicular temperatures. The ion temperatures increase quite dramatically for increasing electric fields; a factor of ~2 increase in temperature for both NO^+ and O^+ results from an electric field of 50 mV/m. Electric fields of the order of 100 mV/m are fairly commonly observed near auroral arcs, and in these cases ion temperatures are expected to be ~4 times their quiescent values. For all electric field values NO^+ has a higher temperature parallel to the geomagnetic field than does O^+. All temperature profiles peak in altitude in the 150–200 km range and then decrease monotonically with altitude above the peak. For both NO^+ and O^+, $T_{s||}$ is smaller than $T_{s\perp}$ at all altitudes. The anisotropy is most pronounced for O^+ above ~200 km.

[14] For a radar beam oriented at small angles to the geomagnetic field, the observed ion line spectra will approximate their typical Maxwellian shape with an effective temperature along the beam line of sight. This line-of-sight temperature, T_s, will be a combination of parallel and perpendicular temperatures [e.g., *Raman et al.*, 1981]:

$$T_s = T_{s\|}\cos^2\phi + T_{s\perp}\sin^2\phi. \quad (5)$$

[15] In equation (5), ϕ is the angle the ISR beam makes with the geomagnetic field. As noted by *Hubert and Lathuillere* [1989] and *Gaimard et al.* [1996] the use of such an approximation in interpreting ISR spectra is appropriate only for $\phi \le 30°$, particularly in situations where $E'_\perp$ is large. Writing the models of equations (2) and (4) in the form $T_{s||} = T_n + \beta_{s||}AE'^2_\perp$ and $T_{s\perp} = T_n + \beta_{s\perp}AE'^2_\perp$, the line-of-sight temperature is

$$T_s = T_n + \left(\beta_{s\|}\cos^2\phi + \beta_{s\perp}\sin^2\phi\right)AE'^2_\perp. \quad (6)$$

2.2. Estimating the Effective Electric Field Magnitude

[16] In order to model ion temperatures self-consistently through equation (6), the effective electric field must be determined. In this work $E'_\perp$ is calculated directly from observed ion temperature profiles in regions of known composition. In the E region (< 150 km altitude), the ions are molecular, and the fitter ion composition correct. Therefore, E region temperature measurements may be used

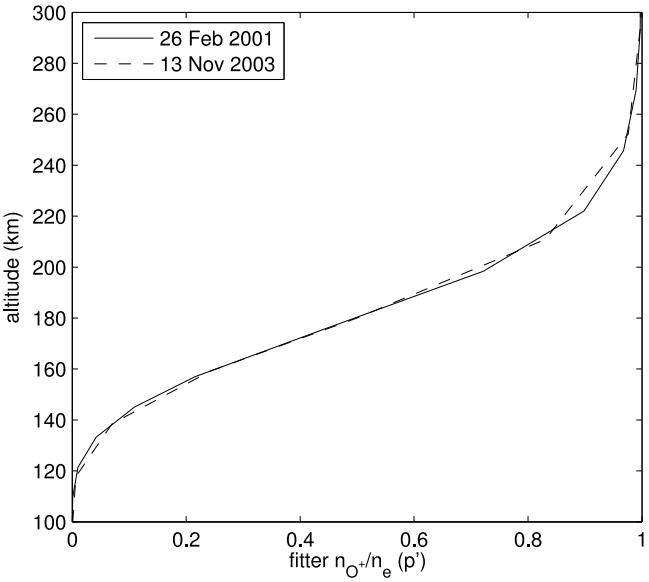

Figure 2. Fitter ion composition profiles, p', for the two case studies used in this work.

with equation (6) to estimate $E'_\perp$. Note that this method implicitly takes the effects of the neutral wind into account (see equation (3)), as opposed to a direct calculation of the electric field through plasma drifts. This point is critical for analysis of temperatures and composition at high latitudes where winds can be substantial during storms [*Richmond and Lu*, 2000] and near discrete auroral features [*St.-Maurice and Schunk*, 1981; *Eastes et al.*, 1992]. It is worth noting that this method of estimating $E'_\perp$ from temperature does require the assumption that $E'_\perp$ does not change with altitude. This assumption hinges on both the electric field ($\mathbf{E}_\perp$) and horizontal wind ($\mathbf{u}_{n\perp}$) being constant with altitude. The former constraint is likely to hold to a high degree of accuracy [e.g., *Kelley*, 2009] while the latter (that $\mathbf{u}_{n\perp}$ is constant with altitude) is more questionable and will be reexamined in section 4.

[17] Using approximations outlined above, there is one unknown ($E'_\perp$) to solve for using reliable T_s measurements from the E region. In this work measurements from the 130–150 km region are used since the temperature gradients below these altitudes are too large to yield a good determination of $E'_\perp$ (e.g., Figure 1). A weighted least squares solution is applied to estimate $E'_\perp$ from measurements at these altitudes for each ion temperature profile.

2.3. Ion Temperature in a Mixed-Species Plasma

[18] As they stand, the models described in section 2.1 are not directly comparable to ion temperatures estimated from IS spectra. The standard method of fitting IS spectra for ion temperature does not actually produce individual estimates of temperature for each ion species in the plasma. Instead the spectral fitting process (as typically applied at high-latitude stations) produces a single temperature which is, in a sense, a species averaged temperature. In a plasma consisting of O^+ and NO^+, ion temperature is approximately given by *Jenkins et al.* [1997]:

$$T_i = p(T_{O^+} - T_{NO^+}) + T_{NO^+}, \tag{7}$$

where T_i is species average temperature in the line-of-sight direction, T_{NO^+,O^+} are line-of-sight temperatures for each individual species, and $p \equiv n_{O^+}/n_e$ is the standard notation for fractional atomic ion content. The actual temperature derived from an IS spectrum is not a simple weighted sum of individual species temperatures, but such an approximation is reasonable in the case of an O^+ and NO^+ plasma.

[19] For a given effective electric field the individual species temperatures can be calculated through the model described in section 2.1. The average ion temperature can therefore be specified as a function of altitude if the composition parameter and effective electric field are known. In subsequent sections we will refer to this ion temperature using the notation $T_i \equiv T_i(z; p)$, which explicitly indicates that this variable has dependence the composition parameter (that we are attempting to estimate) and altitude.

2.4. Formulation of Estimation Technique

[20] The ion composition estimation method is described by the following procedure.

[21] 1. Ion temperature measurements from the 130–150 km region are used to estimate the effective electric field.

[22] 2. The effective electric field is used to model the full line-of-sight temperature profile through equation (6).

[23] 3. This temperature profile is then used to as input to a fitting process (outlined below), thus leaving the ion composition as a free parameter to be estimated.

[24] The high degree of ambiguity between ion temperature and mass allows ion temperatures fitted with a particular ion composition to be mapped to a different composition without having to refit the IS spectrum, as described by *Waldteufel* [1971]. The functions derived by *Waldteufel* [1971] give a means to convert a temperature estimated with $p = 0$ (denoted T_{i0}) to what that temperature would be under a different composition assumption, $p_1 \neq 0$ with corresponding temperature denoted T_{i1}:

$$T_{i1} = F_i(p_1)T_{i0}, \tag{8}$$

where the function F_i is [after *Waldteufel*, 1971]

$$F_i(p) = -2.902 + 0.785p + \frac{8.2}{p + 2.1}. \tag{9}$$

[25] Manipulation of the *Waldteufel* [1971] relations gives the following equation relating true ion temperature T_i (with an unknown true composition p) to temperature derived from the fitter T_i' (with corresponding assumed composition p'):

$$T_i' = \frac{F_i(p')}{F_i(p)} T_i. \tag{10}$$

[26] This equation specifies how much the fitted temperature (T_i') will differ from the true ion temperature (T_i), and will thus form the basis of later minimization procedures to determining the unknown true composition, p. Representative fitter composition profiles (p') for the data sets of interest are shown in Figure 2. In both cases, the composition profiles are representative of quiet conditions with little ion heating. When strong frictional heating is present, the true ion composition is likely to vary from these fitter values

[*Zettergren et al.*, 2010]. It is worth noting that diurnal variations in composition can also be substantial [*Lei et al.*, 2004].

[27] In order to develop a robust estimator of ion composition, this work adopts a reduced parameter description of the ion composition profile. Specifically, the unknown composition profile is assumed to be described by a set of parameters, denoted $\mathbf{x}$. As a result both the modeled ion temperature and $F_i(p)$ coefficient become functions of the parameter set $\mathbf{x}$, i.e., $T_i(z; \mathbf{x})$ and $F_i(z; \mathbf{x})$, respectively. Under this parameterization the true ion composition profile can be found by minimizing the difference between the self-consistently modeled ion temperature and the fitted temperature, adjusted by an unknown composition per equation (10). In the present work, a least squares approach is applied to provide and estimate ($\hat{\mathbf{x}}$) of the parameter set $\mathbf{x}$:

$$\hat{\mathbf{x}} = \arg\min_{\mathbf{x}} \left\{ \sum_k \left[T_i'(z_k) - F_i(p') \frac{T_i(z_k; \mathbf{x})}{F_i(z_k; \mathbf{x})} \right]^2 \right\}. \quad (11)$$

[28] In this expression the index k runs over the different altitudes from a given ion temperature profile measurement.

2.5. Parameterization of the Ion Composition Profile

[29] There have been several attempts to characterize the functional form of $p(z)$, including an empirical representation [*Waldteufel*, 1971] and parameterizations based on physical arguments [*Evans and Oliver*, 1972; *Oliver*, 1975, 1979]. In the present estimation scheme we use a functional form adapted from *Oliver* [1975]:

$$p(z; \mathbf{x}) = \frac{2}{1 + \sqrt{1 + 8 \exp\left(-\frac{z - z_c}{H}\right)}}. \quad (12)$$

[30] For this parameterization $\mathbf{x} = [z_c, H]$, where z_c is the crossover altitude (the altitude at which the plasma is 50% O^+ and 50% molecular ions, and $p = 0.5$) and H is a scale height parameter [cf. *Oliver*, 1975]. This model was developed for use in the midlatitude ionosphere and ostensibly applies to the present problem, with auroral impact ionization playing the role of photoionization. Indeed, this parameterization can be shown to match the essential features of the ion composition profiles simulated by *Zettergren et al.* [2010]. This parameterization is further simplified by adopting $H = 45$ km, since, as shown by *Zettergren et al.* [2010], H is not strongly dependent on applied effective electric field. Thus, for our purposes, we need only to solve for z_c to characterize ion composition during the auroral disturbances.

[31] It is worth noting that this model may not be appropriate in cases of extremely strong precipitation or when electric fields are small. The functional form of ion composition in such cases is probably more complex, but these situations are not of interest to the present research so further analysis is left to future work.

2.6. Physical Constraints for Estimation Procedure

[32] A complicating factor in solving the minimization problem of equation (11) is that model O^+ and NO^+ temperatures differ during frictional heating events (see Figure 1). In particular, $T_{O+||} < T_{NO+||}$ from 200 to 300 km. In some cases of intense heating, this allows the minimization method to fit temperature inversions in the 150–300 km region by using large values for p (indicating a predominantly oxygen plasma). However, the simulations of *Zettergren et al.* [2010] show that intense heating results in mostly NO^+ in this altitude region, and thus should physically eliminate such solutions. In the present work we use the approximation $T_i \approx T_{NO+}$, a constraint which precludes unrealistic solutions corresponding to large p.

[33] It can be shown that the adopted constraint ($T_i \approx T_{NO+}$) is valid for a wide range of realistic heating situations. For small effective electric fields there is little heating and all ion species temperatures are equal, so $T_i \approx T_{NO+}$. For progressively larger values of electric field, p remains small up to higher altitudes so that the average ion temperature (defined by equation (7)) is weighted toward NO^+ temperature. This fact remains true even for highly dynamic frictional heating events. Figure 3 shows comparisons of T_i and T_{NO+} for effective electric fields ranging from 25 to 100 mV/m. These temperature calculations are from the modeling studies published by *Zettergren et al.* [2010], though they were not directly presented in that work. The parallel temperatures are shown here, as they display the largest differences between the species O^+ and NO^+ for a given effective electric field. These calculations show that T_i does not deviate significantly from T_{NO+} for a broad range of electric field values, justifying the constraint $T_i \approx T_{NO+}$.

[34] Minor differences (within typical error bar ranges on temperature fits) between T_i and T_{NO+} in Figure 3 occur only at higher altitudes. To avoid incurring bias in the composition estimates, the altitude domain of the optimization problem of equation (11) is adjusted (based on simulation results of Figure 3) to exclude altitudes where the approximation may yield some systematic error. A final benefit of using model NO^+ temperatures for processing data is that it avoids complications with modeling O^+ temperatures that arise from large uncertainties in O^+-O collision frequency (see discussion by *Oliver and Glotfelty* [1996, and references therein]).

2.7. Filtering of Composition Estimates

[35] The premise of the proposed estimation technique is that the models of equations (2) and (4) are accurate representations of ion temperature behavior. The success of each estimate of ion composition is judged by computing mean square difference between observed ion temperature corrected with the new composition estimate and model calculations of ion temperature. This is compared to the mean square difference between the original temperature observations and ion temperature modeled with the originally assumed ion composition. Estimates for which the mean square data-model difference is larger than the original data-model difference are rejected.

3. Results From Case Studies

[36] Examples of the proposed estimator for various experimental modes are presented below. The data sets are chosen to represent instances of strong ion heating by electric fields (the situation for which the technique was

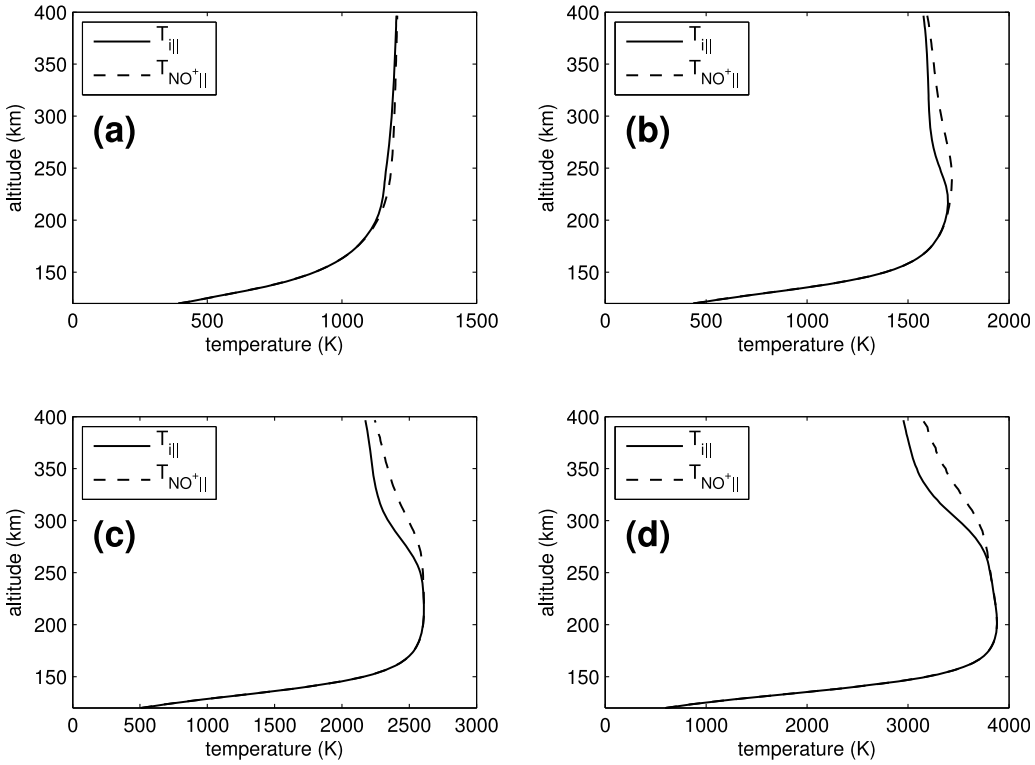

Figure 3. Average parallel ion temperature compared with NO^+ temperature. (a-d) $E'_\perp$= 25, 50, 75, and 100 mV/m, respectively.

designed). Some secondary effects of relative ion-neutral drifts, such as molecular ion upflows and neutral winds, are inferred from these data sets.

3.1. Observations Parallel to B: Sondrestrom ISR, 26 February 2001

[37] At 0215–0415 UT on 26 February 2001 the Sondrestrom ISR was operating in dwell mode in the magnetic zenith and recorded clear evidence of ion heating. Auxiliary camera and radar data show that the ISR was directed at a region adjacent to a weak auroral arc and that this arc was centered on a plasma flow shear [*Zettergren et al.*, 2010]. These conditions remained relatively stable throughout the 0320–0340 UT time period, and represent a situation where composition is expected to vary dynamically. In the present work we extend the analysis of these data by *Zettergren et al.* [2010]. In this experiment, a 160 μs pulse was used and the scattered returns were integrated for 30 s.

[38] Figure 4 shows the results of applying the composition estimation technique to the Sondrestrom 26 February 2001 0215–0415 observations. Figure 4a shows the effective electric field estimated from E region ion temperature, and Figure 4b shows $\widehat{z_c}$ (estimated crossover altitude) as a function of time during the event. Ionospheric composition above Sondrestrom changes dramatically during this event, varying from ~200 km to ~350 km, often over time scales of minutes. In some instances (e.g., during 0315–0345 UT) the F region peak is composed mostly of molecular ions. During most of the 26 February 2001 case study the effective electric field appears to modulate the molecular ion content of the plasma, as expected from previous theoretical work [*Zettergren et al.*, 2010].

[39] Figure 5 shows a comparison of ion and electron temperature estimated by the fitter (T_i' and T_e') and temperatures corrected for variable composition (T_i and T_e). In Figure 5a, the fitter ion temperature displays inversions in the 180–250 km region, characteristic of a wrong fitter composition profile [*Zettergren et al.*, 2010]. Accounting for ion composition in the analysis effectively removes these inversions (Figure 5c). The electron temperature at high latitudes is controlled by more complex mechanisms, precipitating electrons and inelastic cooling collisions, and is more difficult to interpret. However, temperature inversions can occasionally be picked out in the fitter T_e' estimate in Figure 5b.

[40] The intense ion frictional heating during the 26 February 2001 event also produced ionospheric plasma expansion and upwelling which was recorded by the ISR. This ion frictional heating and upwelling process is often referred to in the literature as type 1 upflow [e.g., *Wahlund et al.*, 1992]. An interesting feature of the 26 February 2001 event is that the frictional heating-induced upflow contains very large amounts of NO^+. Figure 6 shows ion temperature (corrected for the estimated ion composition) and upward NO^+ fluxes near the F region peak during the 26 February 2001 case study. As seen in these estimates, enhanced ion temperatures play the dual role of converting the plasma to molecular ions *and* enhancing ion pressure to drive type 1 molecular ion upflows. Peak molecular ion fluxes during the event are quite large, having magnitudes 2–3 $\times$ 10^{13} m^{-2} s^{-1}.

[41] Type 1 upflows shown in Figure 6 are only one class of upflows occurring at ionospheric altitude. Another well-documented process is the type 2 upflow, which is thought to be initiated by *electron* heating processes [*Lynch et al.*,

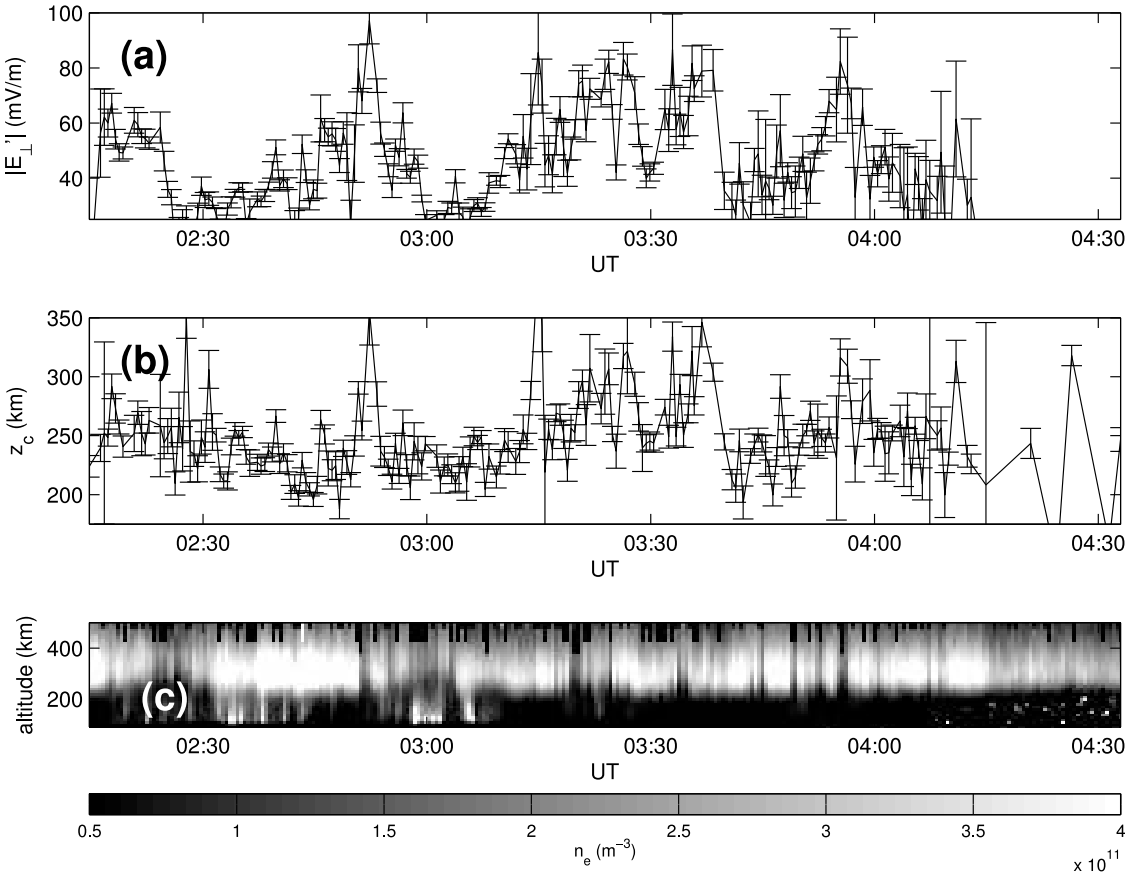

Figure 4. Sondrestrom ISR ion composition case study (26 February 2001): (a) effective electric field, (b) molecular to atomic ion transition altitude, and (c) plasma density.

2007; *Zettergren et al.*, 2007, 2008] followed by plasma expansion and upwelling. Soft precipitating electrons, which deposit their energy near the *F* region peak, drive the electron heating process responsible for the type 2 upflows.

[42] The data presented in this case study suggest an important and fundamental difference between the type 1 and type 2 upflowing plasmas. Type 1 upflows should contain relatively large amounts of molecular ions as compared to type 2 upflows. Frictional heating responsible for type 1 upflows inherently incites production of NO^+ while causing it to expand upward. In contrast, the precipitation responsible for type 2 upflows simply heats the existing *F* region O^+, and likely produces upflow containing mostly O^+. The composition of these ionospheric upflows can also likely be associated with their location in relation to nearby auroral arcs. Inside the area of arc-related precipitation (the upward current region), electric fields are often small, so any upflows will be predominantly O^+. In arc downward current regions electric fields are often quite large [e.g., *Marklund*, 1984; *Johnson et al.*, 1998] and precipitation is weak, so any upflowing plasma will contain comparatively large amounts of molecular ions. It is, however, unclear whether molecular ions fluxes would be more intense than O^+ fluxes in type 1 upflows expected in downward current regions. Future modeling and data analysis should be able to quantify how the composition of upflowing plasma depends on effective electric fields and precipitation.

[43] Several recent studies suggest that high-altitude ion outflow to the magnetosphere may be causally linked to various ionospheric upflow processes discussed above [*Strangeway et al.*, 2005; *Lynch et al.*, 2007; *Ogawa et al.*, 2008]. It is thought that ionospheric upflows deposit large amounts of plasma into higher-altitude regions where other processes like transverse ion heating and parallel potential drops can accelerate the upflowing ions to escape velocity. It therefore seems reasonable to speculate the areas of enhanced molecular ions and upward molecular ion fluxes are source regions for molecular ions that have been observed in the magnetosphere [e.g., *Peterson et al.*, 1994; *Lennartsson et al.*, 2000].

[44] A close inspection of Figure 4 reveals that many of the large enhancements in molecular ions are accompanied by apparent depletions in *F* region plasma density, e.g., ~0250–0300 UT, ~0315 UT, ~0326 UT. These depletions are the result of the fact that NO^+ has a shorter chemical lifetime than O^+. Thus, when a large fraction of the plasma is converted to NO^+, more recombination occurs and depletions form. These depletions likely have important implications for ion upflow resulting from frictional heating. The enhanced recombination of a NO^+ plasma provides a natural negative feedback in the upward flux of molecular ions. The effect this negative feedback has on the amount of upflow produced by frictional heating (type 1) versus upflow from regions of soft precipitation (type 2) is presently unclear. However, the enhanced recombination may be the physical

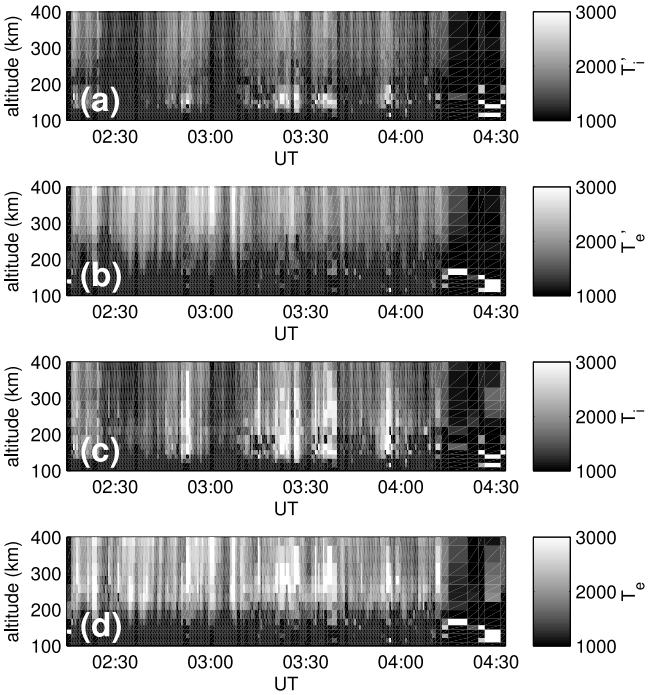

Figure 5. A comparison of ion and electron temperatures estimated by fitter (T_i' and T_e') and temperatures corrected for variable composition (T_i and T_e) for the 26 February 2001 case study: (a) ion temperature from fitter, (b) electron temperature from fitter, (c) ion temperature corrected for composition, and (d) electron temperature corrected for composition.

reason that type 2 upflows are typically more intense than type 1 upflows [*Liu et al.*, 1995]. It may also explain the somewhat lesser correlation of DC Poynting fluxes (as compared to precipitating electrons) to outflowing ion flux [*Strangeway et al.*, 2005].

3.2. Multiple-Beam Observations: Sondrestrom ISR, 13 November 2003

[45] Data recorded on 13 November 2003 by the Sondrestrom ISR included observations of intense ion heating from multiple-beam positions. This experiment includes dwells at three different positions corresponding to azimuth and elevation pairs of (140°,80°), (−99°,70°), (20°,70°). The first position is the magnetic zenith, while the other two dwell positions make an angle of ~26° with the local magnetic field. In this ISR experiment, a 320 μs pulse was used, the scattered returns were integrated for ~3 min at each position. In addition to fitted parameters from each beam position, line of sight velocities from each position are combined to obtain vector velocities (and electric fields) under assumptions of uniformity (see work by *Thayer* [1998] for details).

[46] The use of an experiment with beam positions oblique to the geomagnetic field illustrates an application of the estimation scheme to a data set where ion temperature anisotropies have to be taken into account in the modeling. Figure 7 shows the results of applying the composition estimator to each beam position. Figure 7a shows electric field magnitude measured by combining line-of-sight drifts from all three positions, Figure 7b shows the effective electric field from each beam position, and Figure 7c shows crossover altitude estimated in each beam. As with the previous case study, enhancements in molecular ion content in the ionosphere are correlated with the effective electric field and ion heating. In the present case study there is an extended disturbance in effective electric field from 1130 to 1530 UT. This period is characterized by increases in crossover altitude and significant amounts of NO^+ near the F region peak.

[47] Because the 13 November 2003 experiment mode included direct observations of electric fields as well as estimates of effective electric fields, it offers an opportunity to gather some information about neutral winds. Differences in $E_\perp'$ and $E_\perp$ are attributable to neutral winds as indicated by equation (3). Substituting in $\mathbf{E}_\perp = -\mathbf{v}_{p\perp} \times \mathbf{B}$ into this equation, where $\mathbf{v}_{p\perp}$ is the bulk plasma drift velocity, gives the effective field in terms of relevant drifts:

$$\mathbf{E}_\perp' = -\left(\mathbf{v}_{p\perp} - \mathbf{u}_{n\perp}\right) \times \mathbf{B}. \tag{13}$$

[48] From this equation it can be seen that $E_\perp' < E_\perp$ implies substantial neutral winds along the plasma drift direction, while $E_\perp' > E_\perp$ requires winds in a different direction from the plasma drift.

[49] From Figure 7 it is possible to compare electric field magnitude resolved from the three beam positions (Figure 7a) with the effective electric field measured from each beam (Figure 7b). With a few exceptions, $E_\perp'$ in each beam is approximately equal to $E_\perp'$, implying that the neutral gas is roughly stationary in the Earth-fixed reference frame. Deviations from this pattern are quite interesting. From 1430 to 1530 UT the $E_\perp$ peaks twice at ~100 mV/m, while $E_\perp'$ is constant in all beams at ~50 mV/m. This difference is due to strong neutral winds in the plasma drift direction, which is an expected result of extended collisional

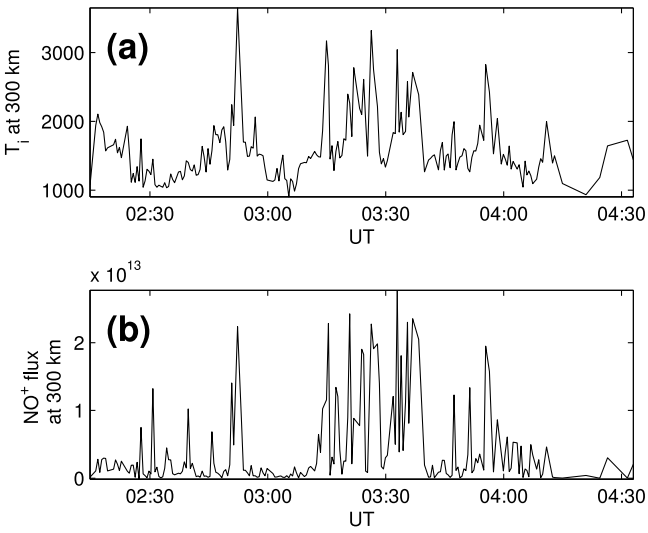

Figure 6. Molecular ion upflow during the 26 February 2001 case study: (a) ion temperature at 300 km altitude corrected for estimated composition and (b) upward NO^+ number flux at 300 km.

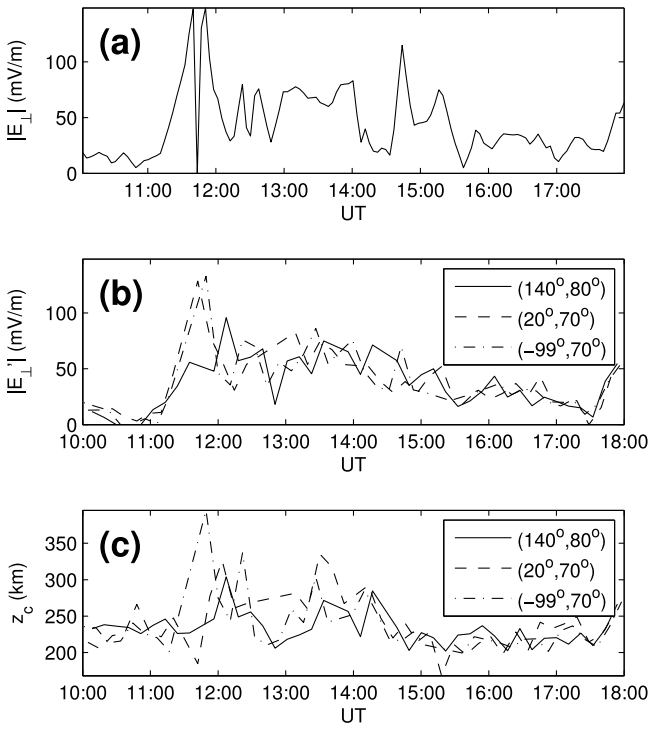

Figure 7. Electric fields versus effective electric fields at 1000–1800 UT on 13 November 2003. (a) Electric field in Earth-fixed reference frame estimated from multiple positive ion drift measurements. (b) Effective electric field estimated from ion temperature in *E* region. (c) Molecular to atomic ion transition altitude, estimated as described in section 2.

momentum transfer between the drifting plasma and neutral gas. Immediately preceding this event, from 1410 to 1430 UT, is a period with $E_\perp$ ~20 mV/m and $E'_\perp$~30–50 mV/m in each beam. This indicates that the neutral wind has a large component in a direction away from the plasma drift.

[50] The occasional differences in $E_\perp$ and $E'_\perp$ in Figure 7 illustrate the important point that the *effective* electric field must be used in modeling the ion temperatures through equations (2) and (4). The electric field in an Earth-fixed frame, $E_\perp$, cannot accurately be used in the analysis of ion energy balance, unless additional measurements of the neutral wind are also available. For example, during 1430–1530 UT we have effective electric fields that differ from the electric field by ≈ 50 mV/m. If $E_\perp$ were used to model ion temperature profile, a drastic overestimate of T_i would result and the proposed minimization scheme (equation (11)) would interpret this incorrectly as a large concentration of molecular ions. In a similar manner, if $E'_\perp$ is used to calculate temperature in situations where $E_\perp < E'_\perp$ then an underestimate of molecular ion content would result. Properly accounting for neutral winds is critical to correctly estimating ion composition.

[51] There are a few significant spatial variations in ion composition during the 13 November 2003 case study. Figure 7c shows ion composition estimated for each beam position during the experiment. Differences in $\widehat{z_c}$ among beams occur during the extended heating from 1130 to 1400 UT. It is unclear what the cause of these differences is, but likely candidates are that the length of time the plasma has been exposed to heating may differ, or that the heating may have significant spatial structure.

3.3. Comparison of Estimates With Numerical Ionospheric Simulations

[52] To evaluate the plausibility of the composition estimates during heating events in the case studies they are directly compared to ionospheric fluid model calculations from the TRANSCAR model [*Blelly et al.*, 1996; *Lilensten and Blelly*, 2002]. TRANSCAR solves the 13 moment transport equations, along geomagnetic field lines [*Blelly and Schunk*, 1993], for seven different ion species: O^+, H^+, N^+, N_2^+, NO^+, O_2^+, and e^-. All temperature-dependent chemistry relevant to the *E* and *F* regions is included in the model [*Diloy et al.*, 1996]. In present comparisons we adopt the results of *Zettergren et al.* [2010], who used TRANSCAR to simulate the response of *F* region ionospheric composition to effective electric fields of varying strength.

[53] Figure 8 shows a scatterplot $\widehat{z_c}$ versus effective electric field during the case study events. The data in this plot consist of the 26 February 2001 0215–0415 UT (circles) and all beam positions from 13 November 2003 at 1000–1800 UT (triangles). Plotted alongside these composition estimates are TRANSCAR simulations for 20 s and 60 s exposure times to an effective electric field. Longer exposure to electric fields will produce progressively larger variations from quiescent composition, but the bulk of the response occurs before 60 s exposure [*Zettergren et al.*, 2010]. In general, the molecular ion content estimated from these case studies is consistent with the TRANSCAR simulations. Scatter in the plot appears to be mostly due to statistical uncertainty, but also probably results from diurnal

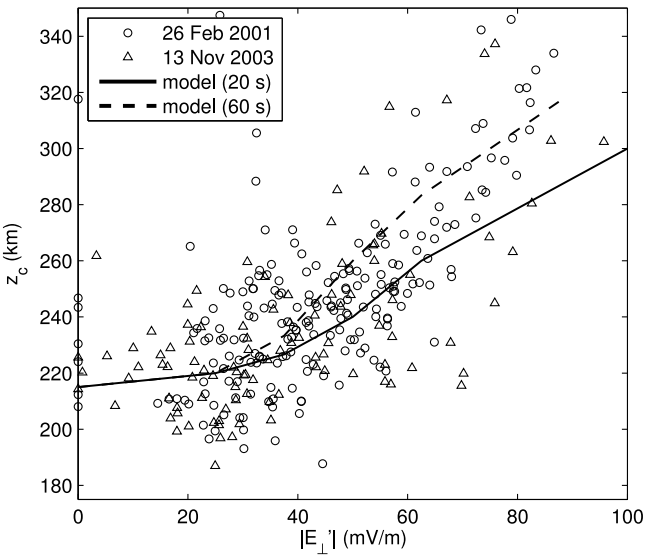

Figure 8. Estimated molecular to atomic ion transition altitude versus effective electric field for the 26 February 2001 0215–0415 UT and 13 November 2003 1050–1800 UT (all beam positions) case studies. Also shown are model calculations adapted from *Zettergren et al.* [2010].

Table 1. Sensitivity of Estimation Technique to Model Input Neutral Atmosphere[a]

Data Set	Beam Position	Error Bar	1/2 O/N_2 $\Delta\widehat{z_c}$	2 O/N_2 $\Delta\widehat{z_c}$	$T_{n\infty}$ = 1300 K $\Delta\widehat{z_c}$	$T_{n\infty}$ = 900 K $\Delta\widehat{z_c}$
26 Feb 2001	mag. Zenith	±13.4	+5.8	−13.1	+18.1	−19.8
13–14 Nov 2003	mag. Zenith	±6.6	+2.7	−5.8	+18.1	−16.4
13–14 Nov 2003	Az 20°, El 70°	±12.8	+4.7	−9.1	+18.7	−15.8
13–14 Nov 2003	Az −99°, El 70°	±11.5	+3.8	−9.5	+17.8	−17.2

[a]All table entries are averages over the entire data set and have units of kilometers.

variability in composition and changes in composition induced by neutral atmospheric O/N_2 variations.

4. Sensitivity Analysis

[54] The main sources of "model error" for the estimation technique are possible variations in the neutral atmosphere from the MSIS values adopted. Here, the robustness of the technique to variations in the neutral atmosphere is evaluated. The possibility of vertical structure in neutral winds, which could affect the accuracy of the proposed technique, is also discussed.

4.1. Sensitivity to O/N_2 and Neutral Temperature Variations

[55] The accuracy of the MSIS neutral atmospheric model will have some effect on the performance of the proposed ion composition estimator. To test the sensitivity to neutral atmosphere variations we run the estimation scheme on the example case studies (from section 3) using neutral atmospheric parameters altered from the MSIS values. Differences between the estimates using MSIS and those using the altered neutral atmospheres give insight into how varying O/N_2 ratios and neutral temperature affect estimates of composition. These differences are quantified in the current discussion as

$$\Delta\widehat{z_c} = \left\langle \widehat{z}_c^{MSIS} - \widehat{z}_c^{ALT} \right\rangle, \tag{14}$$

where $\widehat{z_c}^{MSIS}$ is the crossover altitude estimated using MSIS atmosphere and $\widehat{z_c}^{ALT}$ is the crossover altitude using an altered atmosphere (the specific alterations are discussed below). $\langle\cdot\rangle$ indicates averaging over the entire data set of interest. Such averaging is useful as it yields a single numerical variation in crossover altitude due to altering a particular feature of the neutral atmosphere and easily quantifies estimator behavior. Table 1 shows a summary of results of calculating $\Delta\widehat{z_c}$ for various altered neutral atmospheres, and is the basis of the rest of the discussion in section 4.

[56] The first test of how neutral variations affect the estimator is to alter the O/N_2 ratio while keeping the neutral temperature constant. Neutral composition will have some effect on the model calculations of equations (2) and (4). The average neutral mass $\langle m_n \rangle$ could vary by as much as a factor of roughly two, depending on the altitude, which will affect the temperature profile shape in some way. Results of processing the data sets for various O/N_2 ratios are shown in Table 1. The third column of Table 1 shows the average error bar for each data set processed using the MSIS atmosphere. The fourth and fifth columns show the average variation of crossover altitude (defined by equation (14)) due to altering the MSIS O/N_2 by factors of 1/2 and 2, respectively. For all data sets and O/N_2 ratios, the deviation from the MSIS reference calculations is less than the average error bar. Closer examinations of individual estimates in each data set reveals only minor deviations in $\widehat{z_c}$ estimates when O/N_2 is changed.

[57] A realistic possibility, especially during frictional heating events, is that both the composition and temperature of the neutral atmosphere deviate significantly from MSIS values. To test the robustness of the estimator to simultaneous T_n and O/N_2 variations, the case study data sets are processed using the different model neutral atmospheres shown in the first row of plots in Figure 9. Figures 9a–9c plot O density, N_2 density, and neutral temperature for three different atmospheres: (1) the standard MSIS atmosphere, (2) a heated atmosphere, and (3) a cooler atmosphere. The heated and cooled atmospheres were chosen to represent significant deviations of T_n from reference MSIS values. The exospheric temperature ($T_{n\infty}$) for the cooler atmosphere is 900 K, for the MSIS reference is 1100 K, and for the heated atmosphere is 1300 K. The results of applying the estimation scheme to the 26 February 2001 data sets using each atmosphere are shown in Figures 9d and 9e. Visual inspection reveals that altering the neutral atmosphere produces minor deviations in the estimated effective electric field. The changes in estimated crossover altitude, however, are more substantial. The temporal trends of increasing and decreasing amounts of molecular ions in this event are preserved almost perfectly, even though the estimates are clearly affected by varying the neutral atmosphere. Similar analysis of data spanning 13–14 November 2003 (an extension of the case study period from section 3.2) produced results very much like those shown in Figure 9.

[58] The sixth and seventh columns of Table 1 show average deviations in the value of crossover altitude estimated using atmospheres 2 and 3. These deviations are larger than the average statistical uncertainties, but still of roughly the same magnitude. Of course, larger alterations in the neutral atmosphere from that adopted in the estimator will produce progressively large errors, but the deviations used in this analysis are already quite large. The average differences of 15–20 km are certainly significant, but are preferable to the alternative of simply specifying a static ion composition profile.

[59] The estimator sensitivity to other types of neutral atmospheric variations is quite similar to results summarized in Table 1. Altering the model neutral temperature profile by ±200 K at all altitudes and varying O/N_2 by ±50 % gives errors of slightly lesser magnitude than those shown in the sixth and seventh columns of Table 1.

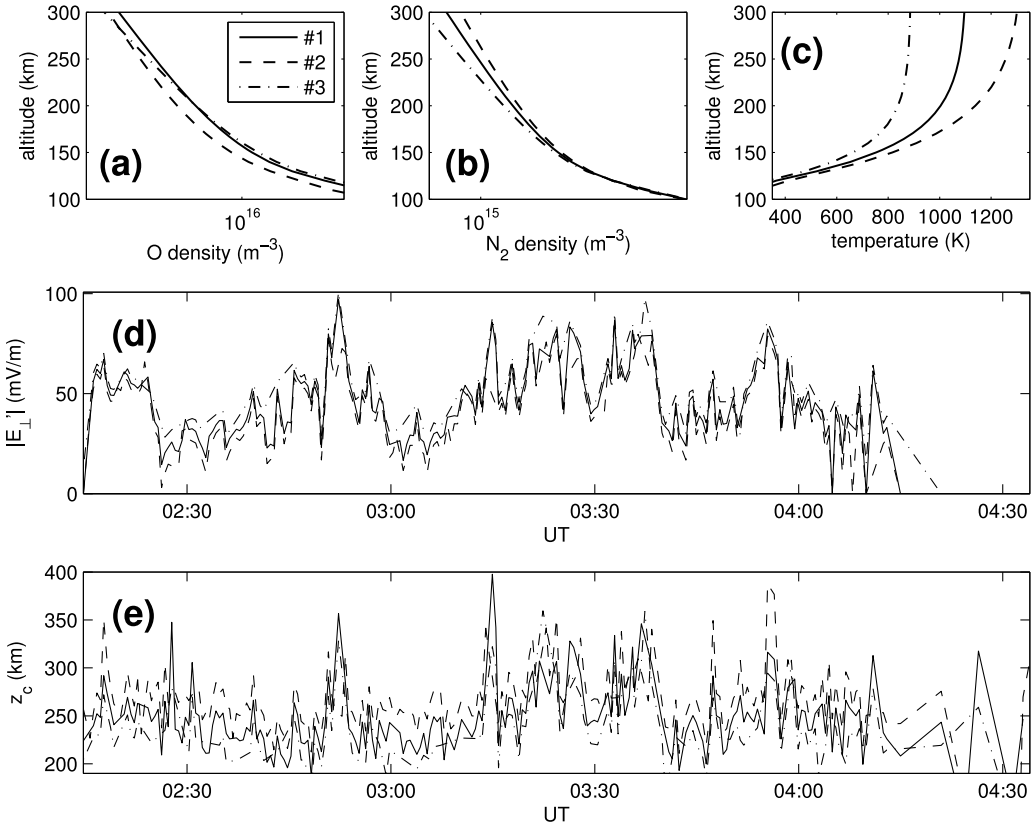

Figure 9. The 26 February 2001 data set processed with three different model neutral atmospheres: (a) oxygen density, (b) molecular nitrogen density, (c) neutral temperature, (d) estimated effective electric field, and (e) estimated molecular to atomic ion crossover altitude. The legend in Figure 9a applies to all plots.

4.2. Neutral Wind Structure

[60] Our case studies above have highlighted the importance of including neutral winds in the analysis, but altitude variability in the winds could also play a significant role in heating events. Specifically, vertical variations in horizontal neutral wind velocity could affect ion temperatures by making the effective electric field altitude dependent (as indicated by equation (3)). This would invalidate an assumption used in the composition estimator: namely, that the effective electric field is constant with altitude. Whether winds have enough structure to affect the technique is unclear, but warrants closer inspection.

[61] Investigating the possible effects of wind structure is difficult since there are few observations of vertical structure in zonal and meridional neutral winds at ionospheric altitudes. *Rino et al.* [1977], *Thayer* [1998], and *St.-Maurice et al.* [1999] have presented compelling evidence of vertical structure in the *E* region based on ISR measurements and analysis of the ion momentum and energy equations. However, these studies have been limited to regions where ion composition in known.

[62] Theoretical studies of wind structure by *St.-Maurice and Schunk* [1981] have shown that strong, sustained ion drifts can produce some structure in neutral wind profiles. In their simulations, a neutral wind component develops in the ion drift direction, a response which would lower the effective electric field (e.g., equation (13)). The neutral wind component in the ion drift direction maximizes around the *F* region plasma density peak, where momentum transfer from the ions to the neutrals is greatest. In terms of ion heating, this type of wind profile would decrease ion temperature at the *F* region peak as opposed to other altitudes. This effect may be significant to the composition estimator, which interprets differences between observed ion temperature and model temperatures (calculated with a constant $E'_\perp$) as being due to variable composition.

[63] Any vertical structure in neutral winds (of the type simulated by *St.-Maurice and Schunk* [1981]) will have a different effect than variable composition on observed ion temperature profiles. Figure 10 illustrates this point using example neutral wind profiles adapted from simulations by *St.-Maurice and Schunk* [1981]. Figure 10a shows typical winds that develop in response to an extended period of strong ion flow. The *x* component of the wind corresponds to the $\mathbf{E}_\perp \times \mathbf{B}$ direction and the *y* component is in the direction opposite to the convection electric field. Figure 10b shows a comparison of model T_i' profiles, calculated under various assumptions, and an average profile (T_i') corresponding to all 26 February 2001 data for which the *E* region effective electric field fell in the range 50–75 mV/m. Each of the model profiles represent what the standard ISR fitter routines would output under various circumstances. Model profile 1 is ion temperature using a constant effective electric field corresponding to observations from 130 to 150 km. Composition is assumed to be correct and altitude variability

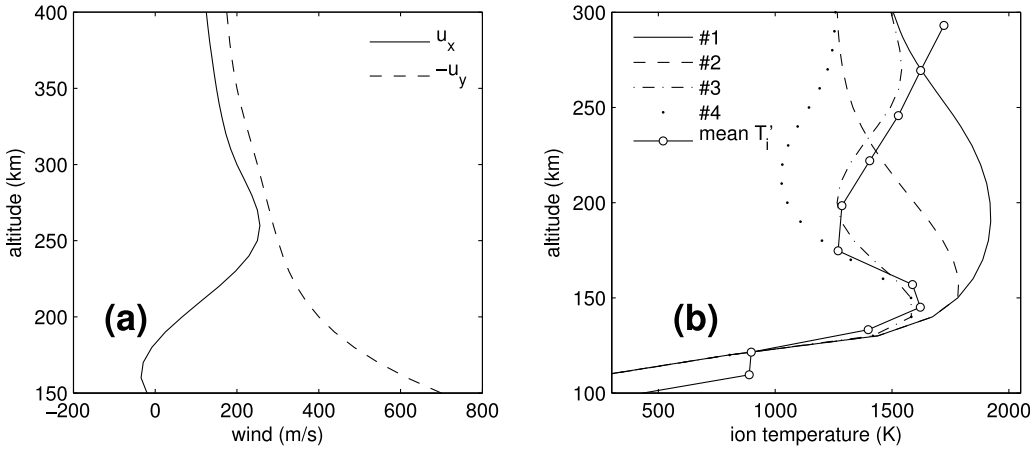

Figure 10. A comparison of average observed temperature profile with model calculations made under different assumptions. (a) Structured wind profiles adapted from *St.-Maurice and Schunk* [1981]. (b) Model calculations and average temperature profile for all 26 February 2001 records having significant heating. Profile 1 was modeled assuming that the fitter composition is correct and that there is no vertical structure in the neutral wind. Profile 2 incorporates an altitude-dependent effective electric field calculated from the wind profiles in Figure 10a. Profile 3 has been adjusted to mimic what the standard fitter routines would output if the true ion composition profile had z_c = 245 km. The effective electric field has been held constant with altitude in profile 3. Profile 4 has been modeled with an altitude-dependent effective electric field and adjusted for a composition profile with z_c = 245 km.

in neutral winds is assumed negligible. Model profile 2 incorporates winds from Figure 10a to model an altitude-dependent $E'_\perp$. Model profile 3 incorporates variable composition estimated from the average observations, but assumes a constant $E'_\perp$ with altitude. Model profile 4 uses an altitude-dependent $E'_\perp$ (again using wind profiles from Figure 10a) and variable composition.

[64] Careful examination of Figure 10 reveals that the observations, on average, do not support the existence of an altitude-dependent wind profile that maximizes near the *F* region peak altitude (~ 300 km for these data). Instead the observed high temperature at 150 km and 300 km, the steep minimum near 200 km, appears support our interpretation of molecular ion enhancements in the 150–250 km range. The apparent temperature minimum around 200 km is consistently the right magnitude to be explained by an incorrect fitter composition profile. It seems unlikely that neutral wind vertical structure can consistently produce these effects. Similar analysis of 13–14 November 2003 data yields the same conclusions.

[65] Time scales associated with wind buildup and composition changes seem to favor the interpretation of structure in ion temperature profiles as being due to an incorrect fitter composition. The vertical wind structure simulated by *St.-Maurice and Schunk* [1981] represents a steady state solution to the fluid equations with a constant ion flow driving the system. In transient situations, the driving ion flow would slowly build the neutral wind up through collisional momentum transfer. The characteristic time scale for this process would be roughly the inverse of the neutral ion collision frequency, probably an hour or longer. For a large fraction of the initial transient period, neutral winds and the effective electric field would contain much less vertical structure than in their final state. This consideration is important because variations in ion composition occur much more quickly. Simulations by *Zettergren et al.* [2010] have demonstrated that large enhancements in molecular ions due to frictional heating occur in as little as 20 s. Thus, variable composition will develop first as a consequence of large ion drifts that later will produce vertically structured neutral winds. This does not rule out the possibility of vertical wind structure, but it does hint that composition variability may be more commonplace.

[66] Aside from arc-driven wind changes, other sources of vertical structure in horizontal winds include atmospheric tides [e.g., *van Eyken et al.*, 2000; *Nozawa et al.*, 2010] and gravity waves [e.g., *Hickey et al.*, 2009]. However, it is unclear whether these processes could have a large effect on horizontal winds at the *F* region altitudes of interest to this paper.

4.3. Incorporating Additional Measurements Into Analysis

[67] The analysis presented in sections 4.1 and 4.2 suggests that if the neutral winds and temperatures are properly constrained, the composition estimator should be accurate (even if O/N_2 is not precisely known). The most straightforward approach to addressing errors due to neutral temperature variations and wind structure would be to incorporate direct measurements into the analysis developed in this work. Fabry-Perot interferometers (FPIs), often used in studying neutral dynamics in the auroral zone [e.g., *Cierpka et al.*, 2000], are capable of resolving neutral temperatures and drifts from multiple-position airglow measurements. However, the derived quantities are representative of the altitude of the emission layer. Untangling the effects of winds, temperatures, and composition in our studies requires knowledge of T_n and $\mathbf{u}_{n\perp}$ at both *E* and *F* region altitudes, so emissions from both these regions are needed. The 557.7 nm and 630.0 nm oxygen emissions, peaking at around 110 km

and 250 km, respectively, are the best candidates for such an analysis. Thus, using multiposition FPI measurements of these airglow/auroral features, one may be able to suitably constrain $T_n(z)$ and $\mathbf{u}_{n\perp}(z)$ and address sources of error in our current analysis. However, this is a substantial project beyond the scope of the current research and is left to future inquiries.

5. Summary and Conclusions

[68] This work has developed a method to estimate ion composition from ISR data during instances of ion frictional heating. The method self-consistently models ion temperature profiles during heating from effective electric field calculations. These modeled temperature profiles are compared to the fitted ion temperature profiles, and differences are interpreted in terms of the ion composition needed to bring the fitted and modeled profiles into agreement. Temperature anisotropies, which are commonplace in auroral regions [*St.-Maurice and Schunk*, 1979], are properly accounted for in the modeling. The composition estimator is applicable to experiments with beam positions at angles of $\phi < 30°$ to the geomagnetic field, where the IS spectra can be interpreted in terms of line-of-sight temperature. Neutral wind effects are partially accounted for through the use of effective electric fields in the model calculations (as opposed to electric fields in the Earth-fixed reference frame). This feature is shown (through analysis of 13 November 2003 data) to be critical to the accuracy of the technique.

[69] The ion composition technique is applied to two example data sets: (1) magnetic zenith observations of ion heating near an auroral arc on 26 February 2001 and (2) multiple-beam-position observations of ion heating and electric fields on 13 November 2003. Results from both case studies demonstrate the expected correlation of ion heating and enhancements of molecular ions driven by the temperature-dependent reaction of equation (1). Intense ion heating adjacent to an auroral arc, during the 26 February 2001 event, is observed to produce large upward fluxes of NO^+ near the F region peak. The 13 November 2003 case study demonstrated the validity of the proposed estimation scheme with measurements oblique to the magnetic field. Substantial neutral winds during this case study are inferred through comparison of electric fields and effective electric fields.

[70] The research presented herein yields the following conclusions and comments.

[71] 1. Estimates of enhanced molecular ions in regions of strong effective electric fields are consistent with theoretical simulations. This result serves to effectively verify the accuracy of the ion composition estimation technique.

[72] 2. Regions of NO^+ upflow adjacent to an auroral arc (in the 26 February 2001 data) are found to be plausible sources for outflowing molecular ions. These type 1 upflows likely have a different ion content than type 2 upflows initiated within auroral arcs.

[73] 3. Effective electric fields during frictional heating events are often quite different from the electric field in the Earth-fixed frame of reference. Thus, it is critical to account for the neutral wind when analyzing ion energy balance.

[74] 4. The composition estimator developed in this work is reasonably robust to neutral atmospheric parameters used in the modeling of ion temperature. Variations in T_n of ± 200 K and O/N_2 of a factor of two from the standard MSIS values produce biases of similar magnitude to statistical uncertainty inherent in the data.

[75] 5. Vertical structure in neutral winds may have a substantial effect on the accuracy of the proposed technique. However, initial data analysis appears to reveal no sustained wind structure during to the case studies presented.

[76] 6. A suitably configured Fabry-Perot interferometer system could likely address most major sources of uncertainty for the proposed technique.

[77] The composition estimator is well suited to studies of upflowing ion composition around auroral arcs, and to indirect studies of the influence of neutral winds on ion composition and density structure. The approach is reminiscent of previous attempts to resolve ion composition in auroral regions [*Häggström and Collis*, 1990], with several very important exceptions. The technique does not require multistatic measurements or multiple-beam positions to function properly, and is therefore suited to experiments with relatively high sampling rates (e.g., 26 February 2001 event used 30 s data). Thus, the method is uniquely qualified to resolve dynamic variations in composition that occur near auroral arcs. Models used in this study are more sophisticated than those used in past attempts to calculate ion composition at high latitudes and include the significant effects of temperature anisotropies and partially account for the influence of neutral winds on ion heating. Last, the validity of the technique is demonstrated through careful comparisons with simulations and thorough error analysis. *Gaimard et al.* [1996] have also used a similar model of ion heating to constrain T_i, but applied their data analysis to individual spectra, instead of focusing on interpretation of entire composition and temperature profiles, as in this work.

[78] **Acknowledgments.** The authors would like to acknowledge Mary McCready for data preparation and the Sondrestrom site crew for campaign support. M.Z. acknowledges the support of NSF grant AGS-1000302 and ERAU internal grant 13267 for this research. M.Z. would also like to thank Bill Oliver for contributing useful discussions and thoughts regarding some of the ideas used in this work.

[79] Robert Lysak thanks the reviewers for their assistance in evaluating this paper.

References

Blelly, P. L., and R. W. Schunk (1993), A comparative study of the time-dependent standard 8-, 13- and 16-moment transport formulations of the polar wind, *Ann. Geophys.*, *11*, 443–469.

Blelly, P.-L., A. Robineau, J. Lilensten, and D. Lummerzheim (1996), 8-moment fluid models of the terrestrial high-latitude ionosphere between 100 and 3000 km, in *Solar Terrestrial Energy Program Ionospheric Model Handbook*, edited by R. W. Schunk, pp. 53–72, Utah State Univ., Logan.

Cabrit, B., and W. Kofman (1997), Ionospheric composition measurement by EISCAT using a global fit procedure, *Ann. Geophys.*, *14*, 1496–1505, doi:10.1007/s00585-996-1496-2.

Cierpka, K., M. J. Kosch, M. Rietveld, K. Schlegel, and T. Hagfors (2000), Ion-neutral coupling in the high-latitude *F*-layer from incoherent scatter and Fabry-Perot interferometer measurements, *Ann. Geophys.*, *18*, 1145–1153, doi:10.1007/s005850000285.

Diloy, P.-Y., A. Robineau, J. Lilensten, P.-L. Blelly, and J. Fontanari (1996), A numerical model of the ionosphere, including the *E*-region above EISCAT, *Ann. Geophys.*, *14*, 191–200.

Eastes, R. W., T. L. Killeen, Q. Wu, J. D. Winningham, W. R. Hoegy, L. E. Wharton, and G. R. Carignan (1992), An experimental investigation of thermospheric structure near an auroral arc, *J. Geophys. Res.*, *97*, 10,539–10,549, doi:10.1029/92JA00168.

Evans, J. (1969), Theory and practice of ionosphere study by Thomson scatter radar, *Proc. IEEE*, *57*, 496–530.

Evans, J. V., and W. L. Oliver (1972), The study of *E*-region ion concentration and composition by incoherent scatter radar, *Radio Sci.*, *7*, 103–112.

Gaimard, P., C. Lathuillere, and D. Hubert (1996), Non-Maxwellian studies in the auroral *F* region: A new analysis of incoherent scatter spectra, *J. Atmos. Terr. Phys.*, *58*, 415–433.

Häggström, I., and P. N. Collis (1990), Ion composition changes during *F*-region density depletions in the presence of electric fields at auroral latitudes, *J. Atmos. Terr. Phys.*, *52*, 519–529.

Hickey, M. P., G. Schubert, and R. L. Walterscheid (2009), Propagation of tsunami-driven gravity waves into the thermosphere and ionosphere, *J. Geophys. Res.*, *114*, A08304, doi:10.1029/2009JA014105.

Hubert, D., and C. Lathuillere (1989), Incoherent scattering of radar waves in the auroral ionosphere in the presence of high electric fields, and measurement problems with the EISCAT facility, *J. Geophys. Res.*, *94*, 3653–3662, doi:10.1029/JA094iA04p03653.

Hubert, D., F. Leblanc, and P. Gaimard (1996), Current state-of-the-art for the measurement of non-Maxwellian plasma parameters with the EISCAT UHF facility, *Ann. Geophys.*, *14*, 1506–1512, doi:10.1007/s005850050412.

Jenkins, B., R. J. Moffett, J. A. Davies, and M. Lester (1997), Nightside ion frictional heating: Atomic and molecular ion temperature anisotropy and ion composition changes, *J. Atmos. Sol. Terr. Phys.*, *59*, 1329–1341.

Johnson, M. L., J. S. Murphree, G. T. Marklund, and T. Karlsson (1998), Progress on relating optical auroral forms and electric field patterns, *J. Geophys. Res.*, *103*, 4271–4284, doi:10.1029/97JA00854.

Kelley, M. C. (2009), *The Earth's Ionosphere: Plasma Physics and Electrodynamics*, 2nd ed., Academic, Amsterdam.

Kelly, J. D., and V. B. Wickwar (1981), Radar measurements of high-latitude ion composition between 140 and 300 km altitude, *J. Geophys. Res.*, *86*, 7617–7626.

Lathuillere, C., and W. Kofman (2006), A short review on the *F*1-region ion composition in the auroral and polar ionosphere, *Adv. Space Res.*, *37*, 913–918, doi:10.1016/j.asr.2005.12.014.

Lathuillere, C., G. Lejeune, and W. Kofman (1983), Direct measurements of ion composition with EISCAT in the high-latitude F_1 region, *Radio Sci.*, *18*, 887–893.

Lathuillere, C., W. Kofman, D. Hubert, and C. La Hoz (1991), Evidence of anisotropic temperatures of molecular ions in the auroral ionosphere, *Geophys. Res. Lett.*, *18*, 163–166, doi:10.1029/90GL02584.

Lei, J., L. Liu, W. Wan, and S.-R. Zhang (2004), Model results for the ionospheric lower transition height over mid-latitude, *Ann. Geophys.*, *22*, 2037–2045.

Lennartsson, O. W., H. L. Collin, A. G. Ghielmetti, and W. K. Peterson (2000), A statistical comparison of the outflow of N_2^+, NO^+ and O_2^+ molecular ions with that of atomic O^+ ions using Polar/TIMAS observations, *J. Atmos. Sol. Terr. Phys.*, *62*, 477–483, doi:10.1016/S1364-6826(00)00019-5.

Lilensten, J., and P.-L. Blelly (2002), The TEC and *F*2 parameters as tracers of the ionosphere and thermosphere, *J. Atmos. Sol. Terr. Phys.*, *64*, 775–793.

Litvine, A., W. Kofman, and B. Cabrit (1998), Ion composition measurements and modelling at altitudes from 140 to 350 km using EISCAT measurements, *Ann. Geophys.*, *16*, 1159–1168.

Liu, C., J. L. Horwitz, and P. G. Richards (1995), Effects of frictional ion heating and soft-electron precipitation on high-latitude *F*-region upflows, *Geophys. Res. Lett.*, *22*, 2713–2716, doi:10.1029/95GL02551.

Lynch, K. A., J. L. Semeter, M. Zettergren, P. Kintner, R. Arnoldy, E. A. MacDonald, E. Klatt, J. LaBelle, and M. Samara (2007), Auroral ion outflow: Low altitude energization, *Ann. Geophys.*, *25*, 1967–1977.

Marklund, G. (1984), Auroral arc classification scheme based on the observed arc-associated electric field pattern, *Planet. Space Sci.*, *32*, 193–211, doi:10.1016/0032-0633(84)90154-5.

McCrea, I. W., M. Lester, T. R. Robinson, J.-P. St.-Maurice, N. M. Wade, and T. B. Jones (1993), Derivation of the ion temperature partition coefficient beta-parallel from the study of ion frictional heating events, *J. Geophys. Res.*, *98*, 15,701–15,715.

McFarland, M., D. L. Albritton, F. C. Fehsenfeld, E. E. Ferguson, and A. L. Schmeltekopf (1973), Flow-drift technique for ion mobility and ion-molecule reaction rate constant measurements. II. Positive ion reactions of N^+, O^+, and H_2^+ with O_2 and O^+ with N_2 from thermal to ~2 eV, *J. Chem. Phys.*, *59*, 6620–6628.

Nozawa, S., et al. (2010), Tidal waves in the polar lower thermosphere observed using the EISCAT long run data set obtained in September 2005, *J. Geophys. Res.*, *115*, A08312, doi:10.1029/2009JA015237.

Ogawa, Y., et al. (2008), Coordinated EISCAT Svalbard radar and Reimei satellite observations of ion upflows and suprathermal ions, *J. Geophys. Res.*, *113*, A05306, doi:10.1029/2007JA012791.

Oliver, W. L. (1975), Models of *F*1-region ion composition variations, *J. Atmos. Terr. Phys.*, *37*, 1065–1076.

Oliver, W. L. (1979), Incoherent scatter radar studies of the daytime middle thermosphere, *Ann. Geophys. C.N.R.S.*, *35*, 121–139.

Oliver, W. L., and K. Glotfelty (1996), O^+-O collision cross section and long-term *F* region O density variations deduced from the ionospheric energy budget, *J. Geophys. Res.*, *101*, 21,769–21,784, doi:10.1029/96JA01585.

Peterson, W. K., T. Abe, H. Fukunishi, M. J. Greffen, H. Hayakawa, Y. Kasahara, I. Kimura, A. Matsuoka, T. Mukai, and T. Nagatsuma (1994), On the sources of energization of molecular ions at ionospheric altitudes, *J. Geophys. Res.*, *99*, 23,257–23,274.

Picone, J. M., A. E. Hedin, D. P. Drob, and A. C. Aikin (2002), NRLMSISE-00 empirical model of the atmosphere: Statistical comparisons and scientific issues, *J. Geophys. Res.*, *107*(A12), 1468, doi:10.1029/2002JA009430.

Raman, R. S. V., J. P. St.-Maurice, and R. S. B. Ong (1981), Incoherent scattering of radar waves in the auroral ionosphere, *J. Geophys. Res.*, *86*, 4751–4762, doi:10.1029/JA086iA06p04751.

Richmond, A. D., and G. Lu (2000), Upper-atmospheric effects of magnetic storms: A brief tutorial, *J. Atmos. Sol. Terr. Phys.*, *62*, 1115–1127, doi:10.1016/S1364-6826(00)00094-8.

Rino, C. L., M. J. Baron, and A. Brekke (1977), High-resolution auroral zone *E* region neutral wind and current measurements by incoherent scatter radar, *J. Geophys. Res.*, *82*, 2295–2304, doi:10.1029/JA082i016p02295.

Schunk, R. W., P. M. Banks, and W. J. Raitt (1975), Effect of electric fields on the daytime high-latitude *E* and *F* regions, *J. Geophys. Res.*, *80*, 3121–3130.

Shibata, T., H. Matsuya, and J. Hoashi (2000), Ion composition in the auroral lower *F*-region inferred from residuals of ion temperature profiles observed with EISCAT, *Adv. Space Res.*, *25*, 201–210, doi:10.1016/S0273-1177(99)00919-9.

St.-Maurice, J.-P., and P. J. Laneville (1998), Reaction rate of O^+ with O_2, N_2, and NO under highly disturbed auroral conditions, *J. Geophys. Res.*, *103*, 17,519–17,522.

St.-Maurice, J.-P., and R. W. Schunk (1979), Ion velocity distribution in the high-latitude ionosphere, *Rev. Geophys.*, *17*, 99–134.

St.-Maurice, J.-P., and R. W. Schunk (1981), Ion-neutral momentum coupling near discrete high-latitude ionospheric features, *J. Geophys. Res.*, *86*, 11,299–11,321.

St.-Maurice, J.-P., and D. G. Torr (1978), Nonthermal rate coefficients in the ionosphere: The reactions of O^+ with N_2, O_2, and NO, *J. Geophys. Res.*, *83*, 969–977, doi:10.1029/JA083iA03p00969.

St.-Maurice, J.-P., C. Cussenot, and W. Kofman (1999), On the usefulness of *E* region electron temperatures and lower *F* region ion temperatures for the extraction of thermospheric parameters: A case study, *Ann. Geophys.*, *17*, 1182–1198.

Strangeway, R. J., R. E. Ergun, Y.-J. Su, C. W. Carlson, and R. C. Elphic (2005), Factors controlling ionospheric outflows as observed at intermediate altitudes, *J. Geophys. Res.*, *110*, A03221, doi:10.1029/2004JA010829.

Thayer, J. P. (1998), Height-resolved Joule heating rates in the high-latitude *E* region and the influence of neutral winds, *J. Geophys. Res.*, *103*, 471–487, doi:10.1029/97JA02536.

Torr, M. R., D. G. Torr, and J. P. Saint-Maurice (1977), The rate coefficient for the $O^+ + N_2$ reaction in the ionosphere, *J. Geophys. Res.*, *82*, 3287–3290.

van Eyken, A. P., P. J. S. Williams, S. C. Buchert, and M. Kunitake (2000), First measurements of tidal modes in the lower thermosphere by the EISCAT Svalbard radar, *Geophys. Res. Lett.*, *27*, 931–934, doi:10.1029/1999GL003687.

Wahlund, J.-E., H. J. Opgenoorth, I. Häggström, K. J. Winser, and G. O. L. Jones (1992), EISCAT observations of topside ionospheric ion outflows during auroral activity: Revisited, *J. Geophys. Res.*, *97*, 3019–3037.

Waldteufel, P. (1971), Combined incoherent-scatter F_1 region observations, *J. Geophys. Res.*, *76*, 6995–6999, doi:10.1029/JA076i028p06995.

Winkler, E., J.-P. St.-Maurice, and A. R. Barakat (1992), Results from improved Monte Carlo calculations of auroral ion velocity distributions, *J. Geophys. Res.*, *97*, 8399–8423.

Zettergren, M. D. (2009), Model-based optical and radar remote sensing of transport and composition in the auroral ionosphere, Ph.D. thesis, Boston Univ., Boston, Mass.

Zettergren, M., J. Semeter, P.-L. Blelly, and M. Diaz (2007), Optical estimation of auroral ion upflow: Theory, *J. Geophys. Res.*, *112*, A12310, doi:10.1029/2007JA012691.

Zettergren, M., J. Semeter, P.-L. Blelly, G. Sivjee, I. Azeem, S. Mende, H. Gleisner, M. Diaz, and O. Witasse (2008), Optical estimation of auroral ion upflow: 2. A case study, *J. Geophys. Res.*, *113*, A07308, doi:10.1029/2008JA013135.

Zettergren, M., J. Semeter, B. Burnett, W. Oliver, C. Heinselman, P. Blelly, and M. Diaz (2010), Dynamic variability in *F*-region ionospheric composition at auroral arc boundaries, *Ann. Geophys.*, *28*, 651–664.

M. Diaz, Electrical Engineering Department, University of Chile, Ave. Tupper 2007, Santiago 8370451, Chile.

C. Heinselman, SRI International, 333 Ravenswood Ave., Menlo Park, CA 94025, USA.

J. Semeter, Department of Electrical and Computer Engineering and Center for Space Physics, Boston University, Boston, MA 02215, USA.

M. Zettergren, Physical Sciences Department, Embry-Riddle Aeronautical University, 600 S. Clyde Morris Blvd., Daytona Beach, FL 32114, USA. (zettergm@erau.edu)